Received: 8 May 2020 | Revised: 11 August 2020 | Accepted: 29 August 2020

DOI: 10.1002/aic.17042

SEPARATIONS: MATERIALS, DEVICES AND PROCESSES

AIChE JOURNAL

FAU zeolite membranes for dewatering of amine-based post-combustion CO_2 capture solutions

Feng Zhu[1] | James Landon[1] | Kunlei Liu[1,2]

[1]University of Kentucky Center for Applied Energy Research, Lexington, Kentucky

[2]Department of Mechanical Engineering, University of Kentucky, Lexington, Kentucky

Correspondence
Kunlei Liu, University of Kentucky Center for Applied Energy Research, Lexington, KY 40511.
Email: kunlei.liu@uky.edu

Funding information
Office of Fossil Energy, Grant/Award Number: DE-FE0031604

Abstract

In amine-based CO_2 capture processes, aqueous amine solvent is circulated between absorber (CO_2 absorption) and stripping (solvent regeneration) columns. To reduce solvent regeneration energy demand, a selective membrane can dewater and enrich the CO_2 concentration in solution prior to the stripper, lowering steam requirements for solution heating. In this work, a facile synthesis strategy was developed to prepare faujasite (FAU) zeolite membranes built upon polydopamine (PDA) modified α-Al_2O_3 substrates. PDA facilitated the attachment of zeolite phases onto the substrate surface to form a 3 μm membrane layer. Membrane permeation flux of 4.45 kg m^{-2} h^{-1} and 95% rejection rate calculated by either CO_2 loading or total alkalinity was achieved in dewatering of CO_2 loaded 30 wt% monoethanolamine (MEA) solution. The effects of temperature on membrane dewatering performance and stability were investigated. This study highlights the potential for process integration of membrane technology in amine-based post-combustion CO_2 capture operations.

KEYWORDS

carbon capture, FAU zeolite membrane, membrane separations, solvent enrichment

1 | INTRODUCTION

CO_2 is often regarded as a primary anthropogenic greenhouse gas. It is imperative to reduce CO_2 emissions from various industrial processes in order to minimize the influence on global climate change. In the last few decades, CO_2 capture technologies have received extensive research and attention to control their emission and storage as well as for a chemical feedstock for utilization.[1,2] Post-combustion capture is currently among the most feasible choices for CO_2 capture because it can be directly used through retrofitting of both coal-fired power plants and natural-gas power plants.[3,4] At present, available post-combustion capture methods include liquid absorption in amine-based solutions, pressure and thermal swing adsorption using zeolites or activated carbons, and gas-phase membrane separations. Among them, the most deeply established and commercially used technology in the industry is based on absorption using aqueous amine-based solutions, which can easily provide >90% CO_2 removal from an atmospheric gas feed stream.[5,6]

However, state-of-the-art CO_2 absorption processes using second generation amines are costly and energy intensive. These costs are due to high capital costs, numerous operational concerns, and notably high energy penalties due to mass transfer limits inside the absorber.[7] In amine-based absorption processes, aqueous amine solvent is circulated between an absorber column for CO_2 absorption and a stripping column for solvent regeneration. The energy requirement for solvent regeneration of state-of-the-art second-generation amine absorption processes varies from 2.2 to 3.0 MJ kg^{-1} CO_2, which contributes to around 80% of the total energy consumption.[8] Such a high energy penalty has driven continuous research towards

This contribution was identified by Lingxiang Zhu (National Energy Technology Laboratory) as the Best Presentation in the session "Advanced Materials for Carbon Dioxide Capture for Power Generation" of the 2019 AIChE Annual Meeting in Orlando.

improving the absorbent performance and enabling the capture step in post-combustion applications to be more economically feasible.[6,9]

Nearly 50% of the total cost of electricity for CO_2 capture is consumed in the capital cost for the construction of the facility with the absorber accounting for the largest single component of this capital cost (15–25%, solvent dependent).[7] It is well accepted that the stripper is equilibrium-controlled while the absorber is mass transfer/diffusion-controlled. For the equilibrium-controlled stripper, the CO_2 loading via CO_2 partial pressure will determine the size of the stripper as well as the energy associated with stripping gases, which typically accounts for approximately 40% of the overall energy required for solvent regeneration. Higher solvent concentrations typically produce higher CO_2 loadings per kilogram of solution at a given temperature compared to a diluted solvent, which would be preferable for stripper applications.[10] However, higher solvent concentrations always correspond to higher viscosities, which will increase the diffusion resistance, thereby reducing mass transfer. To overcome this contradiction, a dewatering membrane can be installed in the rich solvent stream prior to the stripper. During operation, water will preferentially permeate through the membrane and then be pumped back to the absorber, leaving a CO_2 concentrated solution entering the stripper for regeneration and resulting in lower steam requirements to heat up solution, resulting in significant energy savings while not impacting CO_2 absorption rates in the absorber. Integration of a dewatering membrane must be balanced with the overall cost of the system where a higher flux membrane will decrease the capital cost of the membrane component. Due to the nature of the process (decoupling of absorption and desorption active solvent concentrations), the benefits can be broadly applicable to other capture systems where trade-offs exist between mass transfer limitations in the absorber and exorbitant energy regeneration requirements in the stripper.[5,11,12]

Membranes are already reported as process-boosting technology for selected liquid separation processes to increase the CO_2 loading in the rich stream thereby reducing the energy consumption associated with solvent regeneration. Among them, zeolite membranes, especially FAU,[13-15] LTA,[16-18] MFI[19,20] types, have attracted extensive attention in liquid mixture separations such as ethanol/water, isopropanol/water, and dimethyl carbonate/water owing to their well-defined sub-nanometer pore size and thermal, chemical, and mechanical stability.[21,22] Among these zeolites, FAU zeolite membranes with 0.74 nm pore size and 12-membered rings, are well suited for the separation of large molecules which cannot be handled by MFI or LTA with the advantage of its relatively larger pore size. In addition, FAU zeolite membranes display high hydrophilicity due to a relatively low Si/Al ratio of 1–3, which is helpful for the adsorption and diffusion of water molecules, meaning they can be effectively utilized in the dehydration of organic solvents like isopropanol/water, tetrahydrofuran/water, methanol/methyl methacrylate, and ethanol/ethyl tert-butyl ether.[23-25] However, a limited number of studies regarding applying zeolite membranes in the dewatering of amine-based CO_2 capture solutions have been reported.[10] Particularly, there is no report on how to simplify membrane production and ensure high reproducibility for dewatering applications in both commercial and proprietary amine solutions used for CO_2 capture to validate the concept that implementation of selective ceramic membranes prior to the stripper can enrich the CO_2 concentration of amine solution and reduce the energy required in the stripping column.

Recently, a seeding-free strategy for the synthesis of FAU zeolite membranes has been developed to simplify the multistep preparation process that typically involves seeding followed by secondary growth to form a dense and phase-pure membrane layer. Upon treating a porous support material with covalent linker polydopamine (PDA), membrane precursors can be easily anchored via covalent bonds and/or noncovalent adsorption, thus allowing membranes to grow directly on the modified substrates.[26-28]

In the present work, PDA is used to modify the outer surface of α-Al_2O_3 substrates containing a 0.05 μm pore size for the synthesis of FAU zeolite membranes. To further reduce the fabrication cost, easily accessible and soluble sodium aluminate and sodium silicate solutions (water glass) are used as alumina and silica sources, respectively, in the membrane synthesis solution compared to aluminum foil and colloidal silica reported in References 26–28. For the membrane synthesis process, the effect of PDA deposition time was investigated as well as synthesis temperature and time to obtain optimum conditions for a thin, phase-pure, and well inter-grown FAU zeolite membrane on the outer surface of the α-Al_2O_3 substrates. The as-synthesized FAU zeolite membranes were evaluated in the dewatering of CO_2 loaded amine solutions, exhibiting high separation performance and potential for applications in the CO_2 capture industry.

2 | EXPERIMENTAL

2.1 | Synthesis of FAU zeolite membranes

FAU zeolite membranes were prepared on polydopamine-modified α-Al_2O_3 tubes. A 10 mM Tris(hydroxymethyl)aminomethane (Tris–HCl, 99.8%, Sigma-Aldrich) solution was prepared by dissolving Tris–HCl in deionized water. Dopamine hydrochloride (98%, Sigma-Aldrich) was dissolved in the above solution with concentration of 2 mg ml^{-1} in an open glass beaker (diameter: 85 mm). α-Al_2O_3 tubes (I.D./O.D. = 2.9/5.7 mm, L = 100 mm, average pore size ~0.05 μm, Media & Process Technology Inc.) were sealed on both ends with Teflon tape and subsequently immersed in the dopamine solution for surface modification at 25°C with continuous stirring at 300 rpm for a certain time period (0–24 hr) and dried at 45°C for 8 hr, leading to a polydopamine (PDA) layer deposited on the substrate surface. A clear synthesis solution with the molar ratio of 70 Na_2O:1 Al_2O_3:20 SiO_2:2,000 H_2O according to the method reported by Zhou et al[27] was prepared as the membrane synthesis solution. Typically, the aluminate solution was obtained by dissolving 12.86 g sodium hydroxide (97%, Sigma-Aldrich) in 83.33 g deionized water, and then 0.47 g sodium aluminate (50–56% Al_2O_3, 37–45% Na_2O, Sigma-Aldrich) was added to the solution at room temperature and kept stirring for more than 30 min. A mass of 11.77 g sodium silicate solution (26.5% SiO_2, 10.6% Na_2O, 62.9% H_2O, Sigma-Aldrich) was added to the solution dropwise and kept stirring vigorously at 800 rpm for 24 hr at room temperature to produce a clear, homogenous solution. The PDA-modified

α-Al_2O_3 tubes were vertically placed in a Teflon autoclave, and then the synthesis solution was poured into the autoclave. The autoclave was then put into an oven for hydrothermal treatment. After membrane growth under varying time periods (4–20 hr) at different temperatures (80–90°C), the as-synthesized FAU zeolite membrane was washed thoroughly with deionized water and dried overnight in an oven at 70°C for further characterization and dewatering performance tests.

FAU zeolite membranes prepared by the conventional method reported earlier[29] involving dip-coating seeding followed by secondary hydrothermal growth on α-Al_2O_3 tubes were used for comparison in membrane morphology and dewatering performance tests.

2.2 | Solution preparation and analysis

30 wt% monoethanolamine (MEA, 99%, Alfa Aesar) aqueous solution and another proprietary blended amine solution were prepared for membrane dewatering performance tests in this study. The solution for dewatering testing was obtained by introducing a mixture gas of 1.2 L min^{-1} CO_2 and 0.8 L min^{-1} N_2 into 30 wt% MEA solution or proprietary blended amine solution at room temperature for 2 hr to obtain CO_2 loaded amine solution.

The CO_2 loaded amine solutions were analyzed after all additives were fully dissolved. The solution total alkalinity (mol kg^{-1}) was determined by acid titration using the automatic titration instrument Metrohm Titrando 836. In each analysis, the diluted sample was titrated with 0.1 M sulfuric acid until the pH is below 2.5. The volume of the acid at the final equivalence point was used to calculate the alkalinity of the sample. The standard deviation for repeated measurements was ±0.7%. CO_2 content of the loaded solutions was analyzed as described in our previous work.[30-32] Briefly, phosphoric acid liberates CO_2 from CO_2 loaded amine solutions, which is transported by a nitrogen carrier gas to a CO_2 analyzer (HORIBA VIA-510) for quantitative determination. The CO_2 loading value (mol CO_2 kg^{-1} solution) is calculated based on the following equation,

$$\text{Carbon loading}\left(\frac{\text{mol CO}_2}{\text{kg soln}}\right) = \frac{\int_0^t Y_{Co_2}(t)\frac{0.01218F(t)}{T\left(1-Y_{Co_2}(t)\right)}}{m} \quad (1)$$

in which, $Y_{Co_2}(t)$ (%) is the vol% of CO_2 measured by the CO_2 analyzer at time t, $F(t)$ (ml min^{-1}) is the carrier gas (N_2) volumetric flow rate at time t controlled by MFC at standard conditions (e.g., 25°C, 101.325 kPa), and m (kg) is the mass of solution sample.

2.3 | Characterizations

The crystal phases were characterized by powder X-ray diffraction (XRD, Rigaku MiniFlex 600) with a Cu-Kα radiation source in the 2θ range of 5°–50° with an increment of 0.02° per second. The surface and cross-section morphologies of the membranes were observed by scanning electron microscopy (SEM, Hitachi S-4800). For membrane thickness measurement, 10 different locations in the cross-section SEM images were measured and averaged to obtain the final results. The SEM instrument was equipped with energy-dispersive X-ray spectroscopy (EDX, EMAX x-act, Horiba), which was used to determine the bulk Si/Al atomic ratio and elemental compositions of FAU zeolite membranes and particles. The functional groups on FAU zeolite membranes were characterized by ATR-FTIR spectra (Thermo Scientific Nicolet iS-10 FT-IR spectrometer, equipped with attenuated total reflection [ATR] element of Smart iTX AR Diamond). Each spectrum was averaged from 240 scans collected from 400 to 4,000 cm^{-1} at 2 cm^{-1} resolutions. The experiments were run with air as the background, and baseline corrections were applied. Raman spectrum were obtained with a Thermo Scientific Raman Microscope DXR equipped with a ×10 objective lens. Raman measurements were carried out with a laser power of 5 mW and an excitation wavelength of 532 nm. A resolution of 4 cm^{-1} and 64 scans were used in the range of 8–3,562 cm^{-1} for each measurement.

2.4 | Membrane performance evaluation

The dewatering performances for CO_2 loaded aqueous amine solutions through the candidate membranes were evaluated under various operating conditions. Figure 1a shows the schematic diagram of the experimental apparatus used for the testing of membrane dewatering performance. The FAU zeolite membranes were sealed and mounted in a stainless-steel cell with an effective membrane area of 1.54×10^{-3} m^2. The feed solution was heated up and continuously delivered to the membrane module by a prep-pump at a steady flow rate of 30 ml min^{-1}. Dewatering was conducted at temperatures ranging from 110 to 140°C. Pressure of the feed side was adjusted with a back pressure regulator, averaging around 75 psig, which was used as practical stripping column operating pressure in bench studies reported in our previous work.[33] During dewatering process, water content in the CO_2-rich amine solution will preferentially permeate through the membrane, leaving a CO_2 concentrated solution on the retentate side (Figure 1b). The permeate and retentate solutions were condensed with cold trap in an ice bath and analyzed for CO_2 loading and total alkalinity, respectively. The performance of a membrane is expressed as total permeation flux J (kg m^{-2} hr^{-1}) and rejection rate R (%, R_{CL}, rejection rate calculated by CO_2 loading; R_{TA}, rejection rate calculated by total alkalinity), which can be calculated by the following equations:

$$J = \frac{w_p}{A \times t} \quad (2)$$

$$R_{CL} = \frac{CL_f - CL_p}{CL_f} \times 100\% \quad (3)$$

$$R_{TA} = \frac{TA_f - TA_p}{TA_f} \times 100\% \quad (4)$$

Total permeation flux J (kg m^{-2} hr^{-1}) is defined as the mass of permeate produced per unit membrane area per unit time, where w_p

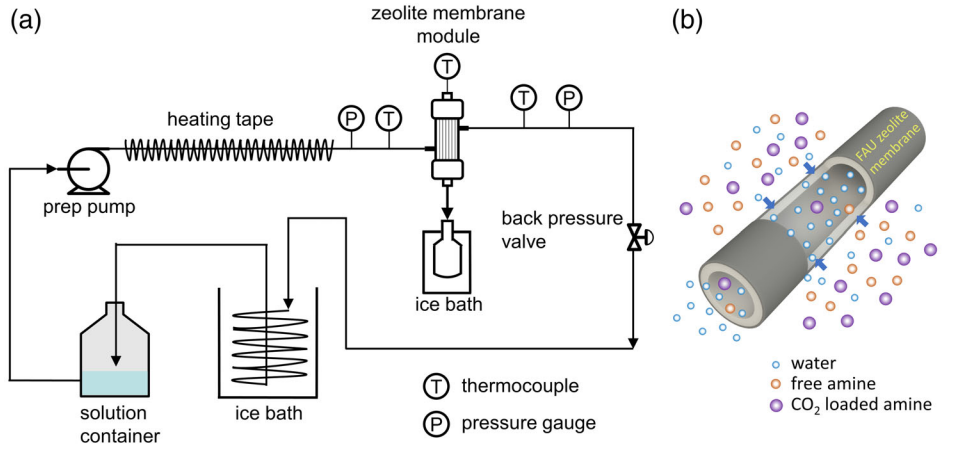

FIGURE 1 Schematic illustration of (a) experimental apparatus for FAU zeolite membrane dewatering performance tests and (b) membrane dewatering process [Color figure can be viewed at wileyonlinelibrary.com]

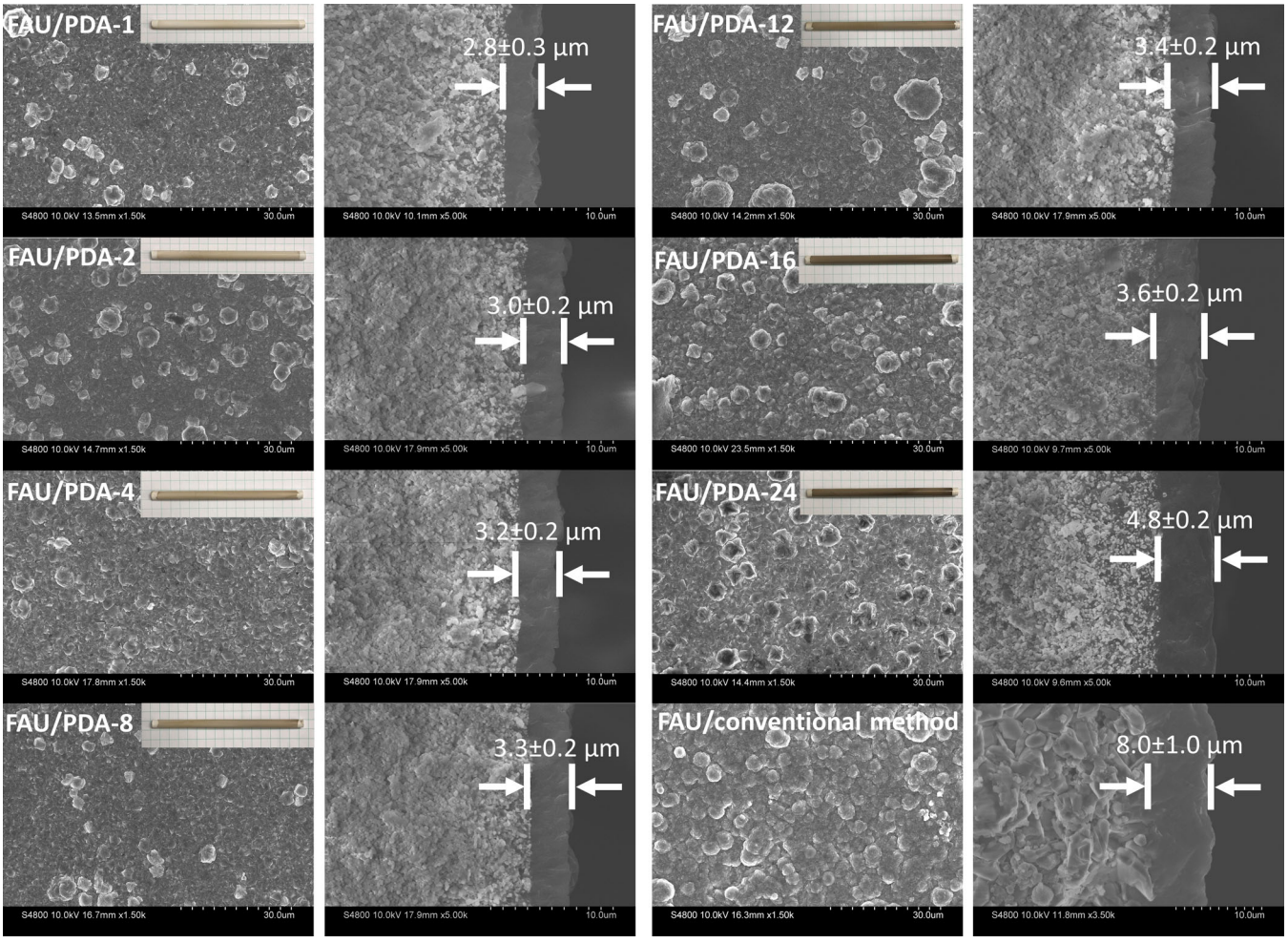

FIGURE 2 SEM images of surfaces and cross-sections of FAU zeolite membranes (FAU/PDA-X) prepared with different PDA deposition times: 1, 2, 4, 8, 12, 16, and 24 hr and inserted pictures of PDA-modified substrates (PDA-X) under corresponding PDA deposition times, compared with a membrane prepared with the conventional seeding-secondary growth method (FAU/conventional method) [Color figure can be viewed at wileyonlinelibrary.com]

(kg) is the weight of the collected permeate solution, A (m^2) is the effective membrane area, and t (hr) is the collection time. R_{CL} and R_{TA} are the rejection rates calculated by the difference in CO_2 loading or total alkalinity in the feed and permeate divided by that in the feed, where CL_f (mol kg^{-1}) is the CO_2 loading of the feed solution, CL_p (mol kg^{-1}) is the CO_2 loading of the permeate solution, TA_f (mol kg^{-1})

is the total alkalinity of the feed solution, TA_p (mol kg^{-1}) is the total alkalinity of the permeate solution. To ascertain the reproducibility of the dewatering performance experimental data, all of the dewatering experiments were repeated on three different membranes synthesized under similar conditions.

3 | RESULTS AND DISCUSSION

3.1 | Effect of PDA deposition time on membrane layer formation

All of the SEM images in Figure 2 were obtained on the as-synthesized FAU zeolite membranes prepared on PDA-modified substrates under a variety of PDA deposition times (1, 2, 4, 8, 12, 16, and 24 hr) with membrane hydrothermal synthesis at 85°C for 11 hr, named as FAU/PDA-X, where X represents the deposition duration. The pictures inserted were taken from PDA modified substrates, named as PDA-X. Prolonged PDA deposition time effectively changed the surface color of the modified substrate from white to dark brown due to the in situ deposition and polymerization of dopamine. In this process, a PDA-rich thin layer with functional groups such as —OH and —NH_2 were quickly formed on the substrate surface. As such, the heterogeneous nucleation of octahedral FAU zeolite crystals on the thin layer of PDA coating forms a dense zeolite membrane layer. It can be seen the substrate surface was completely covered by uniform and compact FAU crystals with no visible cracks, pinholes, or other defects found on the membrane surface. With increasing PDA deposition time, the thickness of the zeolite FAU membranes increased from 2.8 ± 0.3 μm (FAU/PDA-1) to 4.8 ± 0.2 μm (FAU/PDA-24), which indicates the enrichment of zeolite precursors onto the α-Al_2O_3 surface by PDA modification. The functional groups in PDA enhanced the binding force between the grown membrane layer and the substrate, as well as promoting heterogeneous FAU zeolite nucleation.[34,35] Detailed information of FAU/PDA-4 cross-section structure and EDX mapping can be found in Figure S1. The membrane layer was confined to the outer surface of the substrate with barely any infiltration of zeolite/precipitates further into the substrate pores. Membranes synthesized with conventional seeding followed by secondary hydrothermal growth on 1–1.5 μm pore size α-Al_2O_3 substrates were named as FAU/conventional method for comparison. It can be seen that a bumpy surface and thicker membrane layer (8.0 ± 1.0 μm) was formed by this method because the membrane formation induced by nonuniform distribution of zeolite seed particles on the substrate surface.[29] Figure 3 shows the XRD patterns of the as-synthesized FAU zeolite membranes prepared with different PDA deposition times. The formation of FAU zeolite was observed through characteristic peaks[36,37] at 2θ = 6.1°, 10.0°, 15.5°, 23.3°, 26.7°, and 31.0° for all the tested membranes on α-Al_2O_3 (characteristic peaks at 2θ = 26.5°, 35.0°, 37.7°, and 43.2°, JCPDS card 10-0173) substrate. FAU/PDA-4 and FAU/PDA-8 showed identical crystallization peaks to standard FAU, indicating their high crystallinity and purity. By contrast, the loss of peak intensity in FAU/PDA-1 and FAU/PDA-2

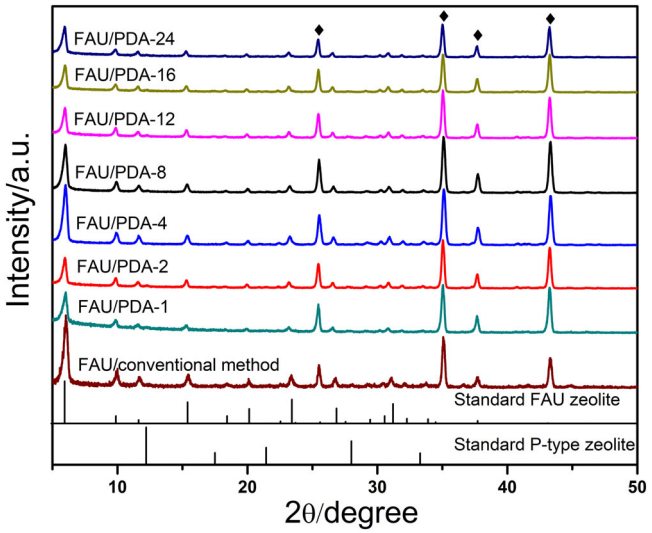

FIGURE 3 XRD patterns of FAU zeolite membranes (FAU/PDA-X) prepared with different PDA deposition time compared with a membrane prepared with the conventional seeding-secondary growth method (FAU/conventional method). ◆, α-Al_2O_3 substrate [Color figure can be viewed at wileyonlinelibrary.com]

demonstrated their incomplete crystallization, which stems from the weaker chelation effect of PDA during zeolite crystal growth. This phenomenon is probably due to one of PDA's special features mentioned above, namely the ability to chelate metal ions. This, in combination with the abundance of metal ions within the synthesis solution, enables PDA to effectively shield its charge, even despite the elevated temperature, and consequently minimizes or even equalizes the otherwise disruptive electrostatic forces between the functionalized support and the charged FAU precursor species.[34] Furthermore, because most of the chelated metal ions are also zeolite building blocks, the functionalized substrate surface now additionally features more direct nucleation points for zeolite layer growth.[38] Together, these two phenomena facilitate nearly unobstructed growth and defect-free membranes.

3.2 | Effect of synthesis temperature and time on membrane formation

FAU zeolite membranes were synthesized on PDA modified α-Al_2O_3 substrates at different synthesis temperatures (80, 85, 90°C) for different time periods (4–20 hr) and named as M1-M14 for different synthesis conditions (Table 1). The structural and morphological evolution of membrane layers are shown in Figure 4. At 80°C, it took a longer time to complete the crystallization process and form a continuous membrane layer. By extending the synthesis time in the range of 8–20 hr, membrane thickness increased from 2.0 ± 0.2 to 3.6 ± 0.2 μm. At 85°C, the membrane thickness increased from 2.8 ± 0.3 to 3.8 ± 0.4 μm when increasing the synthesis time from 8 to 16 hr, along with the appearance of P-type phase at 12 and 16 hr.

TABLE 1 Dewatering performance in CO_2 loaded 30 wt% MEA solution for FAU zeolite membranes (FAU/PDA-4) prepared at different synthesis temperatures and times: 80°C, 8, 12, 16, 20 hr; 85°C, 8, 10, 11, 12, 16 hr; 90°C, 4, 6, 8, 12 hr. Dewatering condition:130°C, 75 psig

No.	Synthesis temperature (°C)	Synthesis time (hr)	Flux (kg m^{-2} hr^{-1})	Rejection rate (CO_2 loading) (%)	Rejection rate (total alkalinity) (%)
M1	80	8	3.29 ± 0.06	70.3 ± 1.2	61.2 ± 0.8
M2	80	12	4.15 ± 0.27	89.8 ± 1.7	89.5 ± 3.3
M3	80	16	3.28 ± 0.16	90.2 ± 3.6	89.1 ± 2.6
M4	80	20	3.30 ± 0.48	92.3 ± 1.0	92.0 ± 2.6
M5	85	8	2.61 ± 0.19	92.3 ± 1.7	94.3 ± 1.5
M6	85	10	4.03 ± 0.22	92.2 ± 1.2	93.6 ± 2.3
M7	85	11	4.45 ± 0.43	94.8 ± 1.4	95.0 ± 0.9
M8	85	12	2.54 ± 0.34	94.8 ± 1.4	93.7 ± 2.3
M9	85	16	1.88 ± 0.08	89.9 ± 1.3	88.0 ± 2.2
M10	90	4	3.23 ± 0.15	91.5 ± 1.5	92.4 ± 3.0
M11	90	6	2.55 ± 0.38	93.1 ± 1.8	94.2 ± 2.2
M12	90	8	2.78 ± 0.45	91.7 ± 0.4	93.1 ± 0.8
M13	90	12	1.66 ± 0.09	86.5 ± 8.5	83.6 ± 10.5
M14[a]	90	9	3.35 ± 0.23	94.1 ± 1.3	96.8 ± 1.4

[a]M14, FAU zeolite membrane prepared with conventional seeding method.

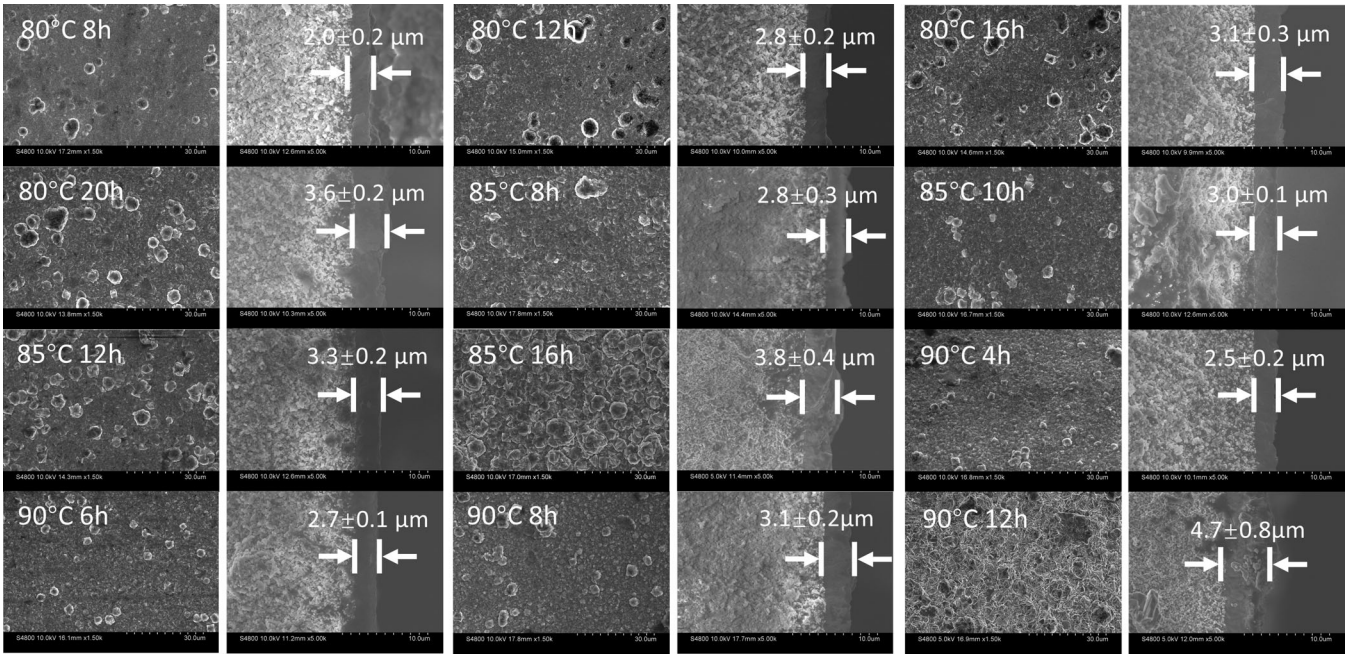

FIGURE 4 SEM images of the surface and cross-section of FAU zeolite membranes (FAU/PDA-4) prepared with different synthesis temperatures and times: 80°C, 8, 12, 16, 20 hr; 85°C, 8, 10, 12, 16 hr; 90°C, 4, 6, 8, 12 hr

Characteristic peaks occurring at 2θ = 12.5°, 17.7°, 21.7°, 28.2°, and 33.4° indicates the existence of P-type foreign phase zeolite[36,39] due to more aggressive competitive crystal growth. At 90°C, it can be seen that compact and continuous FAU membranes were formed on the substrate surface even in 4 hr, although with less sharp zeolite crystals. With increasing crystallization time from 4 to 12 hr, membrane layer thickness continuously increased from 2.5 ± 0.2 to 4.7 ± 0.8 μm. P-type phase was found at 12 hr as well (Figure 5). P-type zeolite is thermodynamically more stable than FAU-type zeolite, but its crystallization requires a long induction period because the nucleation rate is slower than that of FAU-type.[40] Consequently, longer synthesis times exceeding 12 hr were not appropriate in this case. The membranes M1,

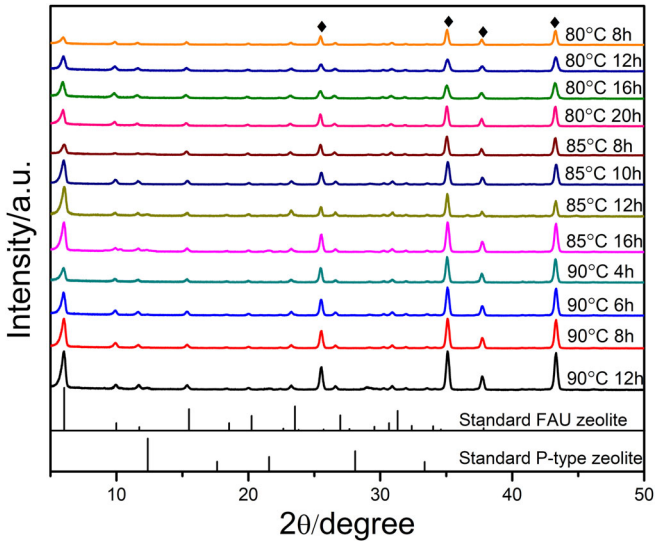

FIGURE 5 XRD patterns of FAU zeolite membranes (FAU/PDA-4) prepared at different synthesis temperatures and times: 80°C, 8, 12, 16, 20 hr; 85°C, 8, 10, 12, 16 hr; 90°C, 4, 6, 8, 12 hr. ♦, α-Al_2O_3 substrate [Color figure can be viewed at wileyonlinelibrary.com]

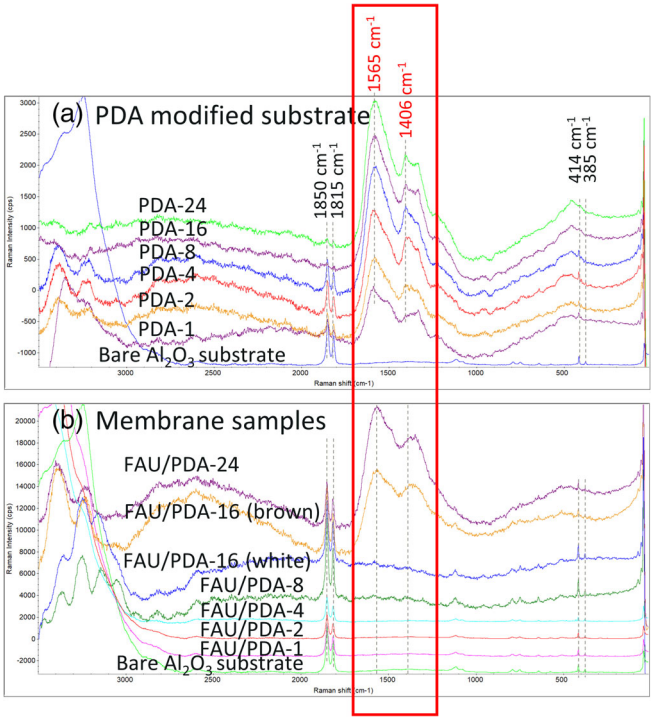

FIGURE 6 Raman spectra of (a) α-Al_2O_3 substrates modified with different PDA deposition time (PDA-X) and (b) FAU zeolite membranes (FAU/PDA-X) prepared on substrates modified with dopamine for 1, 2, 4, 8, 16, and 24 hr [Color figure can be viewed at wileyonlinelibrary.com]

M5, M12 and M2, M8, M13 were synthesized for the same time period (8 and 12 hr) at different temperatures (80, 85, and 90°C). By using the same synthesis time of 8 hr, the membrane thickness increased from 2.0 ± 0.2 μm (M1) to 3.1 ± 0.2 μm (M12) with an increase of synthesis temperature, also showing enhanced characteristic peak intensity in the XRD patterns. Figure 4 shows an increase of membrane thickness from 2.8 ± 0.2 μm (M2) to 4.7 ± 0.8 μm (M13) was also found by comparing membranes using the same synthesis time of 12 hr, however, higher temperature 85 and 90°C caused more obvious formation of P-type impurity structures,[16,41] which is in good agreement with the increase of P-type zeolite characteristic peak intensity in Figure 5.

3.3 | Raman characterization

The experimental Raman spectrum of both series of PDA-modified α-Al_2O_3 substrates (PDA-X) and as-synthesized FAU zeolite membranes (FAU/PDA-X) are shown in Figure 6. The bare Al_2O_3 substrate showed characteristic peaks of Al_2O_3 at 414, 1815, and 1850 cm^{-1}. PDA-X samples showed the presence of two broad characteristic peaks at 1406 and 1,565 cm^{-1} (caused by stretching vibration and deformation of the catechol group), in addition to a few intrinsic peaks of Al_2O_3. The intensity of the catechol group peaks considerably increased upon PDA deposition time, signifying coating of a thicker PDA layer onto the Al_2O_3 substrate. After the membrane synthesis, most catechol group peaks disappeared except for the FAU/PDA-16 and FAU/PDA-24 samples. Both white and brown areas can be visually seen on the FAU/PDA-16 membrane and confirmed with different spectra (Figure S2). The catechol group peaks appeared in brown areas on FAU/PDA-16 and FAU/PDA-24, indicating that the PDA layer remains on the substrate, while the white areas showed similar spectra as other samples without catechol group peaks. Since the membrane thickness is 2.8–4.8 μm, it is speculated that longer PDA deposition times resulted in a thicker PDA layer on the substrate surface, which can be detected within the detection limit of Raman spectrum.[42,43] The membrane synthesis process consumed certain thickness of the grafted PDA layer, thus forming a different interface between membranes and substrates, which may have affected the membrane dewatering performance.

3.4 | Application of FAU zeolite membranes in dewatering of CO_2 loaded amine solution

The FAU zeolite membranes prepared on substrates with PDA from different deposition times were examined for dewatering in CO_2 loaded 30 wt% MEA solution (CO_2 loading = 2.2–2.4 mol kg^{-1}, total alkalinity = 4.2–4.4 mol kg^{-1}) and a proprietary blended amine solution (CO_2 loading = 2.4–2.6 mol kg^{-1}, total alkalinity = 5.3–5.6 mol kg^{-1}) for flux and rejection rate performance (Figure 7). FAU/PDA-0, indicating in-situ FAU zeolite membrane grown on alumina tubes without modification of PDA, exhibited the lowest flux and rejection rate among all of the samples. This lower flux was due to infiltration of zeolite crystals into the substrate pores during the formation of the membrane layer. The lower rejection rate resulted from defects formed during random growth of the membrane layer on the substrate surface. When PDA deposition time was increased from 0 to

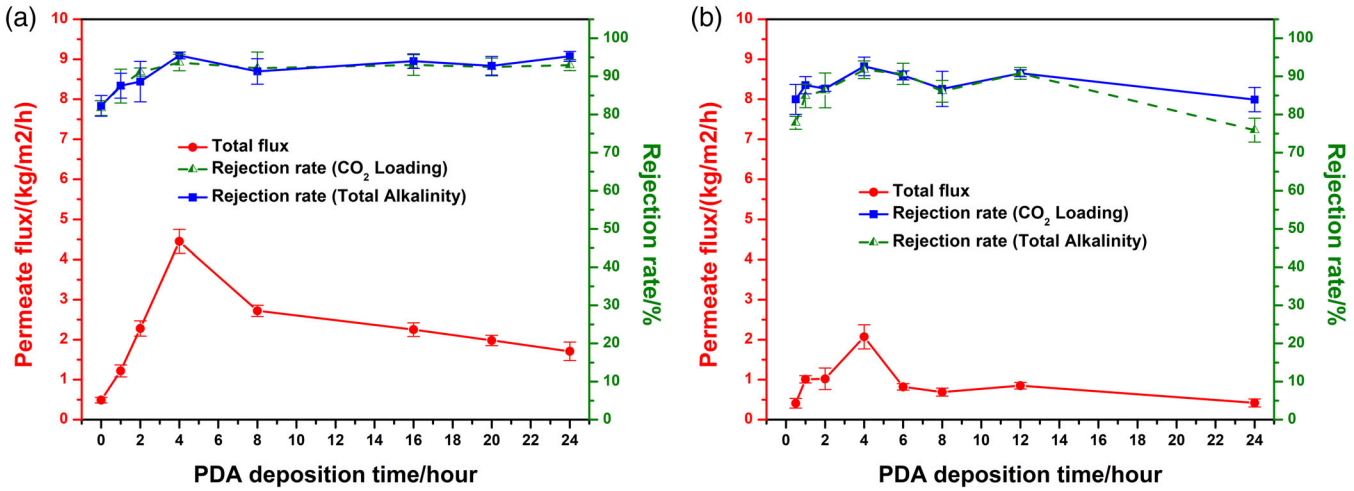

FIGURE 7 Dewatering performance in CO_2 loaded (a) 30 wt% MEA solution (b) proprietary blended amine solution for FAU zeolite membranes (FAU/PDA-X) as a function of PDA deposition time. Dewatering condition: 130°C, 75 psig [Color figure can be viewed at wileyonlinelibrary.com]

4 hr, both flux and rejection rate increased. This result indicated that the membrane became more ordered and contained fewer defects. The highest membrane flux of 4.45 ± 0.43 kg m^{-2} h^{-1} with rejection rate of 94.8 ± 1.4% calculated by CO_2 loading and 95.0 ± 0.9% calculated by total alkalinity were achieved when PDA deposition time was 4 hr. As the deposition time increased further from 4 to 24 hr, the flux dropped mainly due to the increase in the membrane thickness and membrane density, resulting in more permeation resistance. However, a high rejection rate above 90% was maintained. Other control experiments have been conducted on bare α-Al_2O_3 substrate and substrate after PDA deposition for 4 hr (Table S1). When tested in CO_2 loaded 30 wt% MEA solution at 130°C, 75 psig, they can achieve fluxes of 1791.1 ± 5.6 kg m^{-2} hr^{-1} and 1700.2 ± 3.7 kg m^{-2} hr^{-1} with rejection rates of 1.9 ± 0.7% and 3.6 ± 0.9% calculated by CO_2 loading, respectively.

Dewatering performance of FAU zeolite membranes (FAU/PDA-4) prepared at different synthesis temperatures and times were compared using CO_2 loaded 30 wt% MEA solution (Table 1). The dewatering performance of these membranes showed a trade-off between flux and rejection rate. Among all the membranes, preparation at 85°C for 11 hr achieved the best balance in dewatering performance, which is consistent with the membrane morphology and structure shown in Figures 2 and 4. M14 is the FAU zeolite membrane prepared with a conventional seeding method. The thicker and denser membrane layer resulted in lower flux and higher rejection rate.

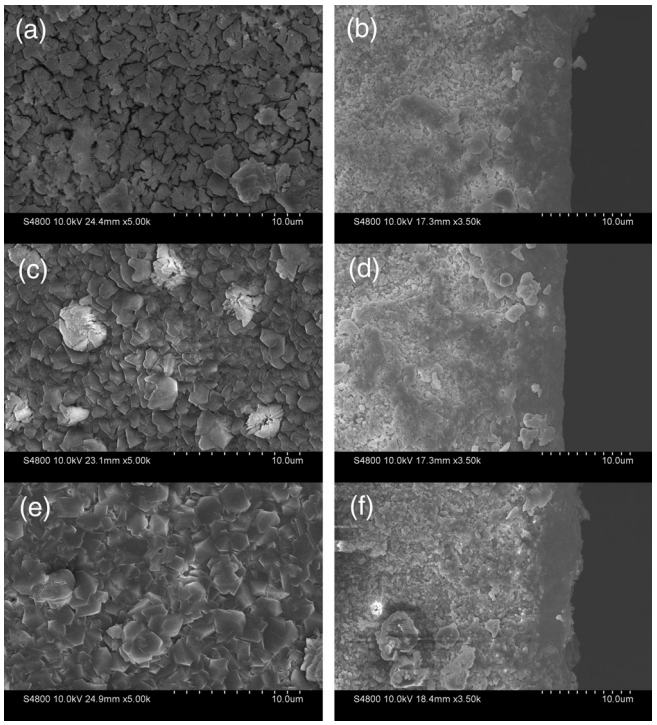

FIGURE 8 Membrane morphology after stability testing at 120°C for 2 hr in (a and b) deionized water; (c and d) CO_2 loaded 30 wt% MEA solution; (e and f) CO_2 loaded proprietary blended amine solution

3.5 | Membrane stability

3.5.1 | Effect of solvent used for dewatering test

Stability testing was carried out on FAU zeolite membranes (FAU/PDA-4 synthesized at 85°C for 11 hr) to investigate their potential for long-term applications. The membrane stability was compared in three solutions: (a) deionized water, water content = 100 wt %, pH = 7.0; (b) CO_2 loaded 30 wt% MEA solution, water content = 60–65 wt%, pH = 8.9; (c) CO_2 loaded proprietary blended amine solution, water content = 40–45 wt%, pH = 9.2. In all stability tests, membranes from the same batch were immersed in Teflon vessels with 90 ml solution maintained at 120°C with autogenic pressure for 2 hr, named as M15, M16, and M17, respectively. The Si/Al atomic ratio of the as-synthesized membrane surface is 0.94 ± 0.01.

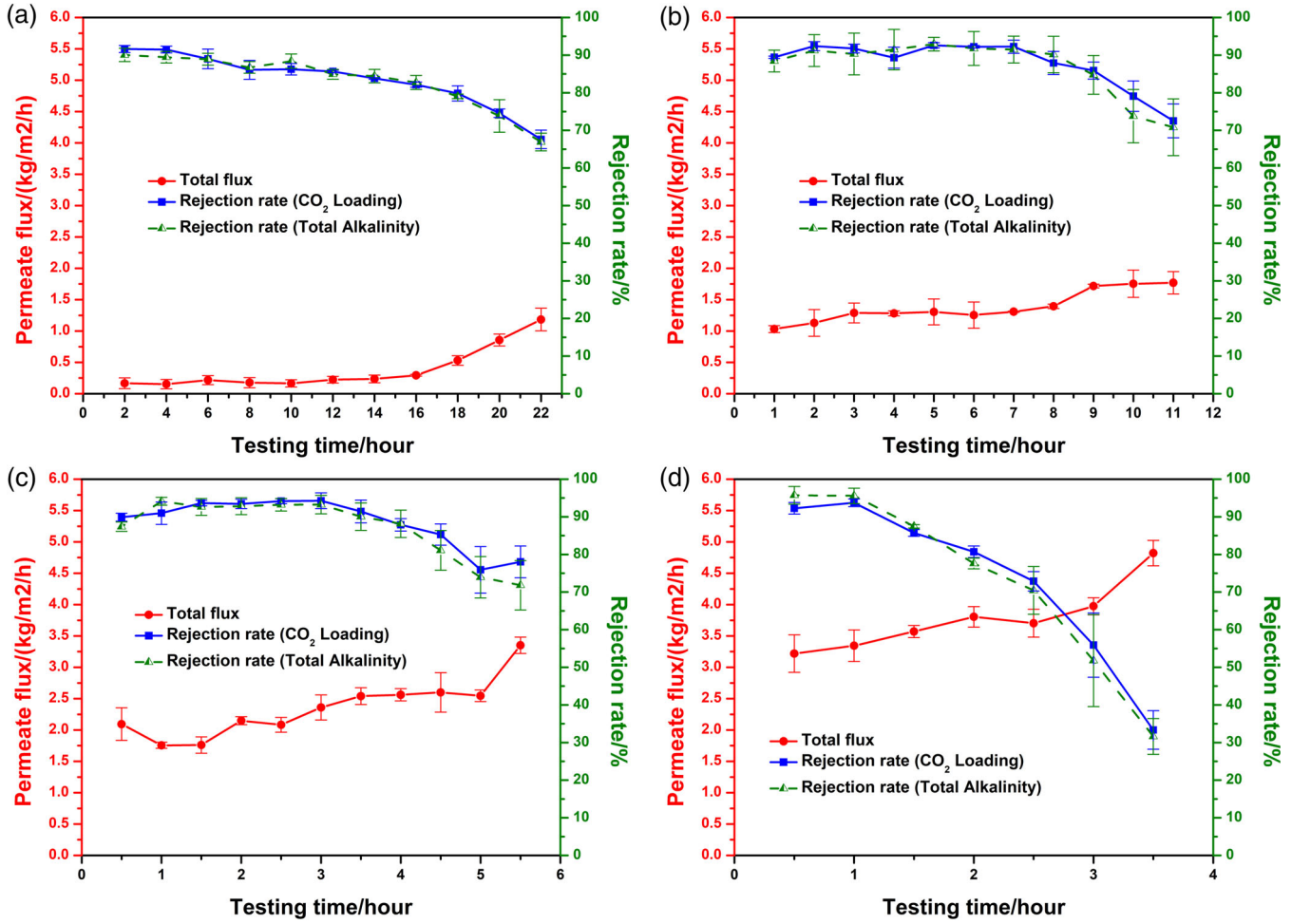

FIGURE 9 Dewatering performance stability tests of FAU zeolite membranes (FAU/PDA-4) at (a) 110°C; (b) 120°C; (c) 130°C; (d) 140°C with 75 psig pressure in CO_2 loaded proprietary blended amine solution [Color figure can be viewed at wileyonlinelibrary.com]

Figure S1c,d shows the EDX mapping of membrane cross-section area and line scan results at two locations along the membrane thickness. The interface between the membrane and the support can be clearly identified. The cross-sectional Si/Al ratio indicated by line scan was consistent (0.93 ± 0.17 and 0.94 ± 0.13) with the membrane surface (0.94 ± 0.01). The SEM images of M15 treated with deionized water (Figure 8a,b) indicated a distinct change for external crystal morphology, from the typical octahedral crystals to a pitted surface, consistent with the morphology of FAU membrane (Si/Al = 1.4) immersed in 50/50 wt% IPA/water mixture at 130°C, 42 hr reported by Sawamura et al.[23] A significant Si/Al ratio decrease from 0.94 ± 0.01 to 0.42 ± 0.10 was measured on the membrane surface (Table S2). However, a lower degree of membrane damage was found in post-treatment solvents with lower water content. Modest change of zeolite crystal edges can be seen in M16 treated with CO_2 loaded 30 wt% MEA (Figure 8c,d). The Si/Al ratio decreased to 0.66 ± 0.04. The morphology of zeolite remained almost unchanged after the treatment with a CO_2 loaded proprietary blended amine solution on M17 (Figure 8e,f). The Si/Al ratio decreased slightly to 0.81 ± 0.06. It was reported that under water rich conditions, the degradation of the crystallinity of NaA zeolite due to its low Si/Al ratio around 1 makes NaA membranes unstable for the long-term dehydration of organic solutions with high feed water content.[23] The main degradation mechanism is suggested to be hydrolysis of the siloxane bonds (Si—O—Si), which starts at terminal Si—OH groups because of their strong interaction with water molecules and hydroxyl ions, leading to the formation of amorphous material.[44] Density of silanol defects plays a crucial role in determining susceptibility of zeolites to hot liquid water.[45] The EDX spectra also indicated the existence of nitrogen in M16 (4.52 ± 0.34%) and M17 (2.38 ± 0.46%), likely due to contamination of the amine in the damaged membrane areas. The severity of membrane damage was in the order of M17 < M16 < M15. That is to say, the membrane stability may be affected by both water content and amine.

3.5.2 | Effect of temperature

Temperature is another significant factor in determining the longevity of membranes during the dewatering process and the adsorption loading and diffusivity of components in the membrane layer, which affects the membrane separation performance. FAU/PDA-4 membranes synthesized at 85°C for 11 hr were tested for dewatering of a

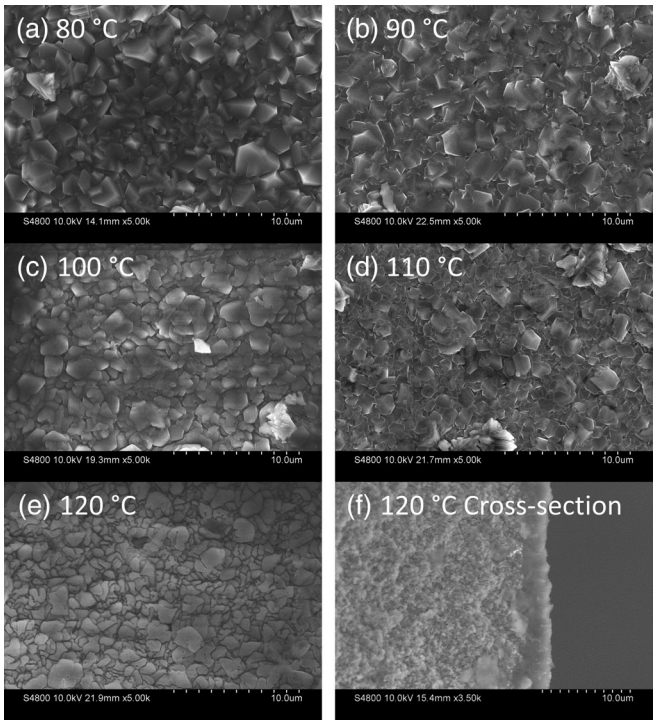

FIGURE 10 SEM images of membrane surface and cross-section area of FAU/PDA-4 membranes after the 120 hr stability testing at temperatures from 80 to 120°C in the CO_2 loaded proprietary blended amine solution

CO_2 loaded proprietary blended amine solution. This blended solvent contains other benefits in the CO_2 capture process compared to a 30 wt% MEA solution, such as higher stability and CO_2 carrying capacity, but also a higher viscosity (nearly ×4–5 the viscosity). Shown below in Figure 9, the flux and rejection rate were tracked as a function of time at 110–140°C. As expected, the higher temperature was beneficial for improving the membrane flux. When the dewatering test temperature was increased from 110 to 140°C, membrane flux increased from 0.20 kg m^{-2} hr^{-1} up to 3.48 kg m^{-2} hr^{-1} while the rejection rate remained stable. It can be explained that, higher temperature increased the saturation fugacity partial pressure of water on the feed side, which enhanced its driving force for permeation through the membrane; additionally, the self-diffusion coefficient of water was also accelerated at higher temperatures.[46,47] The rejection rate was above 80% during the first 18, 10, 5, and 2 hr for membranes tested at 110, 120, 130, and 140°C, respectively. After that, the rejection rate decreased to below 80% while membrane flux showed an increasing trend. This suggests a significant increase in pore size as a result of the long-term test, which may have altered the microporosity of the membranes.

The morphology of FAU zeolite membranes (from the same batch of FAU/PDA-4 synthesized at 85°C for 11 hr) were compared at different temperatures from 80 to 120°C in a CO_2 loaded proprietary blended amine solution. Membranes from the same batch were immersed in Teflon vessels with 90 ml solution maintained at 80–120°C with autogenic pressure for 120 hr, named as M18-22. The SEM images in Figure 10 clearly displayed significant alteration of the membrane layer upon amine solution treatment with increased temperature. M18 treated at 80°C showed sharp crystals (Figure 10a) nearly the same as the as-synthesized membrane M7 (Figures 2 and S1) for surface section with Si/Al of 0.91 ± 0.04. M19 treated at 90°C showed a slightly flattened surface with Si/Al of 0.79 ± 0.07. When the treatment temperature was increased to 100 and 110°C, obvious membrane morphology damage started to appear. The Si/Al ratios dropped to 0.58 ± 0.04 (M20) and 0.57 ± 0.09 (M21), which were lower than M16 (0.66 ± 0.04) treated with CO_2 loaded 30 wt% MEA at 120°C for 2 hr. Figure 10e of M22 treated at 120°C showed a distinct change in crystal morphology after stability testing with a Si/Al ratio of 0.51 ± 0.05, which was much lower than the Si/Al ratio of M17 (0.81 ± 0.06) treated in the same solution at 120°C for 2 hr. However, the damage was not found in the cross-section (Figure 10f). The effect of treatment temperature in amine solution on the resulting Si/Al ratio in Table S3 indicates that a higher temperature led to preferential dissolution of silica sites over alumina sites, showing increased rate of change in Si/Al ratio. The additional difference in the Si/Al ratio was less than 0.1 on membranes treated above 100°C, which indicates further increases in the temperature did not result in a proportional loss of Si. The final value of the Si/Al ratio after the stability test was 0.51 ± 0.05 within 120 hr. Therefore, while the rate of change in the Si/Al ratio can be accelerated at increased operating temperature, there is a limit to the total loss in Si under these conditions. This phenomenon can be explained by easier Si—O—Si bond breakage in comparison to Si—O—Al bond breakage in an alkaline medium. Si-O-Al bonds in high aluminum zeolites are not as labile as the Si—O—Si under basic conditions and cannot rearrange the structure so as to incorporate mesoporosity.[48] The decrease of bulk Si/Al molar ratio was caused by elimination of silicon-rich extra-framework species while the dissolving of zeolitic framework was inhibited by octahedral extra-framework Al species, especially for zeolites with Si/Al < 3.[49,50] The fact that Al is more difficult to extract can be explained by the negative charge associated with Al tetrahedra in the zeolite framework, hindering its extraction of Al through hydrolysis of Si-O-Al bonds by negatively charged hydroxyl groups.[51,52] The negative impact of high temperature on the membrane integrity by accelerating desilication in the membrane layer correlates well with the evolution of the dewatering performance in Figure 9, as damage of the zeolite membrane layer leads to enhanced water flux at the expense of membrane rejection rate.

To figure out whether the membrane damage is a result of collapse of the zeolite crystal framework or intercrystal boundaries destruction, the stability of zeolite particles was also investigated in the CO_2 loaded proprietary blended amine solution for comparison. A mass of 1 g commercial ZEOLYST CBV100 FAU type zeolite and 1 g zeolite particles collected from the synthesis solution after hydrothermal treatment at 85°C for 11 hr (named as FAU-p) were placed in Teflon vessels with 90 ml solution maintained at 120°C with autogenic pressure for 120 hr. SEM, XRD, and EDX analyses were gathered before and after stability testing. Shown in Figure 11, no significant difference was seen in either the particle morphology

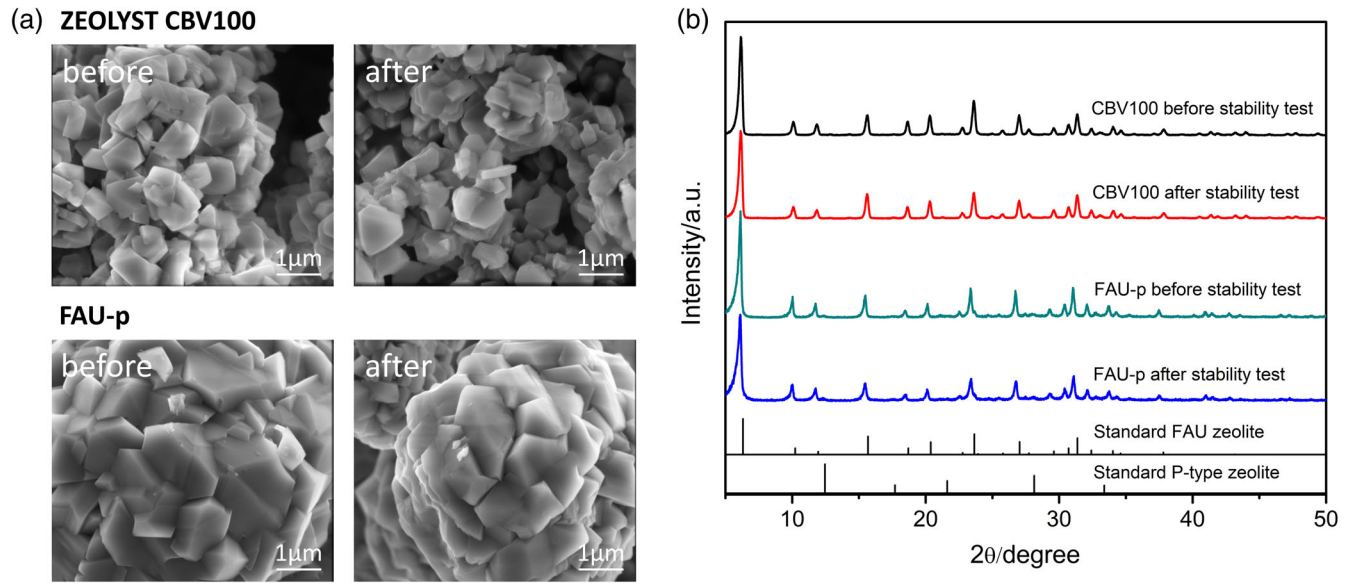

FIGURE 11 (a) SEM images and (b) XRD patterns FAU zeolite particles before/after stability tests at 120°C for 120 hr in the CO_2 loaded proprietary blended amine solution [Color figure can be viewed at wileyonlinelibrary.com]

or the XRD patterns. Table S4 shows the Si/Al ratio slightly decreased from 2.46 ± 0.18 to 2.42 ± 0.09 for ZEOLYST CBV100 and 1.09 ± 0.01 to 1.05 ± 0.03 for FAU-p particles after treatment in amine solution, indicating that the FAU zeolite crystal structure was stable under these conditions. Attenuated total reflectance/Fourier transform infrared spectroscopy (ATR/FTIR) has been used to characterize as-synthesized FAU zeolite membranes and post treated membranes after stability tests (Figure S3). The broadened peaks in the range of 1,000–500 cm^{-1} indicated the amorphization of aluminisilicate structures was enhanced by higher water content and temperature.[53-55] Therefore, it is postulated that the selective removal of Si from the membrane layer as well as dissolution of membrane intercrystal boundaries is responsible for damage of the membrane layer and degradation of membrane performance during the dewatering process of amine-based aqueous solutions. Previous work has demonstrated the existence of high-density amorphous phases at the grain boundary between zeolite crystallites,[53,56] and the high-density amorphous aluminosilicate could be easily dissolved in alkaline solutions by preferential removal of Si species while less dissolvable Al species were retained.[57] The resultant damage of the zeolite membrane layer by alteration of the intercrystal boundaries accordingly increased membrane flux and decreased the rejection rate.

Hence, there is a requirement to build zeolite membranes that can oppose degradation in amine-based aqueous solution at high temperature. Potential alternative pathways to address this problem could include post-treatment by functionalization with organosilanes that serve as a protection layer, as suggested by Zhang et. al,[45] which can prevent water attack by reducing the reactivity of silanol groups. A similar strategy has been applied on hydrophobic all-silica DD3R membranes by enhancing the surface hydrophilicity,[58] showing good stability in the pervaporation dehydration of acidic solutions. Although the increase of stability may negatively impact the membrane flux, this strategy may provide future directions to enhance the stability of zeolite membranes for this dewatering application.

4 | CONCLUSION

In summary, FAU zeolite membranes have been successfully prepared by PDA modification on α-Al_2O_3 substrates for dewatering of amine-based post-combustion CO_2 capture solutions. A properly designed PDA modification method as an interfacial molecular bridge to covalently anchor the membrane precursors was used here, contributing to a dense and pure phase FAU zeolite membrane with a thickness of approximately 3 μm. After comparing the dewatering performance, a synthesis condition with 4 hr PDA deposition, synthesized at 85°C for 11 hr was chosen. The best FAU zeolite membrane exhibited a flux up to 4.45 kg m^{-2} hr^{-1} and a rejection rate, calculated by either CO_2 loading or total alkalinity, above 95% at 130°C, 75 psig. Selective removal of Si species from the membrane layer as well as dissolution of membrane intercrystal boundaries is responsible for damage of the membrane layer and degradation of membrane performance during the dewatering process of amine-based aqueous solution. The as-developed FAU zeolite membranes pave a way towards additional applications for membrane technology in the CO_2 capture industry.

ACKNOWLEDGMENTS

The authors are grateful to the U.S. Department of Energy for project funding (No. DE-FE0031604). The authors also thank Mr. R. Perrone for help in designing and constructing the membrane cells. Rosemary Calabro, David Eaton, and Doo Young Kim are appreciated for their support in the Raman characterization. Nicolas Briot is gratefully acknowledged for EDX characterization. This contribution was

identified by Lingxiang Zhu (National Energy Technology Laboratory) as the Best Presentation in the session "Advanced Materials for Carbon Dioxide Capture for Power Generation" of the 2019 AIChE Annual Meeting in Orlando.

ORCID

Feng Zhu https://orcid.org/0000-0001-9680-9231

REFERENCES

1. Olajire AA. CO_2 capture and separation technologies for end-of-pipe applications–a review. *Energy*. 2010;35(6):2610-2628.
2. Mondal MK, Balsora HK, Varshney P. Progress and trends in CO_2 capture/separation technologies: a review. *Energy*. 2012;46(1):431-441.
3. Wang M, Lawal A, Stephenson P, Sidders J, Ramshaw C. Post-combustion CO_2 capture with chemical absorption: a state-of-the-art review. *Chem Eng Res Des*. 2011;89(9):1609-1624.
4. Raynal L, Bouillon P-A, Gomez A, Broutin P. From MEA to demixing solvents and future steps, a roadmap for lowering the cost of post-combustion carbon capture. *Chem Eng J*. 2011;171(3):742-752.
5. Rochelle GT. Amine scrubbing for CO_2 capture. *Science*. 2009;325(5948):1652-1654.
6. Dutcher B, Fan M, Russell AG. Amine-based CO_2 capture technology development from the beginning of 2013. A review. *ACS Appl Mater Interfaces*. 2015;7(4):2137-2148.
7. James III, PhD RE, Kearins D, et al. *Cost and Performance Baseline for Fossil Energy Plants Volume 1: Bitumonous Coal and Natural Gas to Electricity*. United States: NETL; 2019.
8. Ahn H, Luberti M, Liu Z, Brandani S. Process configuration studies of the amine capture process for coal-fired power plants. *Int J Greenhouse Gas Control*. 2013;16:29-40.
9. Chowdhury FA, Yamada H, Higashii T, Goto K, Onoda M. CO_2 capture by tertiary amine absorbents: a performance comparison study. *Ind Eng Chem Res*. 2013;52(24):8323-8331.
10. Li X, Remias JE, Neathery JK, Liu K. NF/RO faujasite zeolite membrane-ammonia absorption solvent hybrid system for potential post-combustion CO_2 capture application. *J Membr Sci*. 2011;366(1–2):220-228.
11. Wang C, Luo H, De J, Li H, Dai S. Carbon dioxide capture by superbase-derived protic ionic liquids. *Angew Chem Int Ed*. 2010;49(34):5978-5981.
12. Qi G, Liu K, House A, et al. Laboratory to bench-scale evaluation of an integrated CO_2 capture system using a thermostable carbonic anhydrase promoted K_2CO_3 solvent with low temperature vacuum stripping. *Appl Energy*. 2018;209:180-189.
13. Zhou H, Korelskiy D, Leppäjärvi T, Grahn M, Tanskanen J, Hedlund J. Ultrathin zeolite X membranes for pervaporation dehydration of ethanol. *J Membr Sci*. 2012;399:106-111.
14. Zhou J, Zhou C, Xu K, Caro J, Huang A. Seeding-free synthesis of large tubular zeolite FAU membranes for dewatering of dimethyl carbonate by pervaporation. *Microporous Mesoporous Mater*. 2020;292:109713.
15. Zhu F, Peng L, Yao X, Zhang Y, Zhang C, Gu X. Hollow-fiber-supported gold and zirconium-doped faujasite catalytic membranes for hydrogen purification. *Energ Technol*. 2017;5(12):2283-2293.
16. Okamoto K-i, Kita H, Horii K, Kondo KT. Zeolite NaA membrane: preparation, single-gas permeation, and pervaporation and vapor permeation of water/organic liquid mixtures. *Ind Eng Chem Res*. 2001;40(1):163-175.
17. Sato K, Nakane T. A high reproducible fabrication method for industrial production of high flux NaA zeolite membrane. *J Membr Sci*. 2007;301(1–2):151-161.
18. Liu D, Zhang Y, Jiang J, Wang X, Zhang C, Gu X. High-performance NaA zeolite membranes supported on four-channel ceramic hollow fibers for ethanol dehydration. *RSC Adv*. 2015;5(116):95866-95871.
19. Korelskiy D, Leppäjärvi T, Zhou H, Grahn M, Tanskanen J, Hedlund J. High flux MFI membranes for pervaporation. *J Membr Sci*. 2013;427:381-389.
20. Wu Z, Zhang C, Peng L, Wang X, Kong Q, Gu X. Enhanced stability of MFI zeolite membranes for separation of ethanol/water by eliminating surface Si–OH groups. *ACS Appl Mater Interfaces*. 2018;10(4):3175-3180.
21. Noack M, Kölsch P, Schäfer R, Toussaint P, Caro J. Molecular sieve membranes for industrial application: problems, progress, solutions. *Chem Eng Technol*. 2002;25(3):221-230.
22. Lai Z, Bonilla G, Diaz I, et al. Microstructural optimization of a zeolite membrane for organic vapor separation. *Science*. 2003;300(5618):456-460.
23. Sawamura K-i, Furuhata T, Sekine Y, Kikuchi E, Subramanian B, Matsukata M. Zeolite membrane for dehydration of isopropylalcohol–water mixture by vapor permeation. *ACS Appl Mater Interfaces*. 2015;7(25):13728-13730.
24. Zhou R, Zhang Q, Shao J, Wang Z, Chen X, Kita H. Optimization of NaY zeolite membrane preparation for the separation of methanol/methyl methacrylate mixtures. *Desalination*. 2012;291:41-47.
25. Zhu M, Huang S, Gong Y, et al. Effect of flouride on preparation and pervaporation performance of NaY zeolite membrane for EtOH/ETBE mixture. *Microporous Mesoporous Mater*. 2019;282:48-52.
26. Liu Q, Wang N, Jr C, Huang A. Bio-inspired polydopamine: a versatile and powerful platform for covalent synthesis of molecular sieve membranes. *J Am Chem Soc*. 2013;135(47):17679-17682.
27. Zhou C, Yuan C, Zhu Y, Caro J, Huang A. Facile synthesis of zeolite FAU molecular sieve membranes on bio-adhesive polydopamine modified Al_2O_3 tubes. *J Membr Sci*. 2015;494:174-181.
28. Zhou C, Zhou J, Huang A. Seeding-free synthesis of zeolite FAU membrane for seawater desalination by pervaporation. *Microporous Mesoporous Mater*. 2016;234:377-383.
29. Gu X, Dong J, Nenoff TM. Synthesis of defect-free FAU-type zeolite membranes and separation for dry and moist CO_2/N_2 mixtures. *Ind Eng Chem Res*. 2005;44(4):937-944.
30. Zheng L, Landon J, Zou W, Liu K. Corrosion benefits of piperazine as an alternative CO_2 capture solvent. *Ind Eng Chem Res*. 2014;53(29):11740-11746.
31. Matin NS, Remias JE, Neathery JK, Liu K. Facile method for determination of amine speciation in CO_2 capture solutions. *Ind Eng Chem Res*. 2012;51(19):6613-6618.
32. Liu K, Jinka KM, Remias JE, Liu K. Absorption of carbon dioxide in aqueous morpholine solutions. *Ind Eng Chem Res*. 2013;52(45):15932-15938.
33. Frimpong RA, Johnson D, Richburg L, et al. Comparison of solvent performance for CO_2 capture from coal-derived flue gas: a pilot scale study. *Chem Eng Res Des*. 2013;91(6):963-969.
34. Mundstock A, Wang N, Friebe S, Caro J. Propane/propene permeation through Na-X membranes: the interplay of separation performance and pre-synthetic support functionalization. *Microporous Mesoporous Mater*. 2015;215:20-28.
35. Jiang X, Li S, Bai Y, Shao L. Ultra-facile aqueous synthesis of nanoporous zeolitic imidazolate framework membranes for hydrogen purification and olefin/paraffin separation. *J Mater Chem A*. 2019;7(18):10898-10904.
36. Treacy MM, Higgins JB. *Collection of Simulated XRD Powder Patterns For Zeolites Fifth (5th) Revised Edition*. Amsterdam: Elsevier; 2007.
37. Fan F, Feng Z, Li G, Sun K, Ying P, Li C. In situ UV Raman spectroscopic studies on the synthesis mechanism of zeolite X. *Chem–Eur J*. 2008;14(17):5125-5129.

38. Mundstock A, Friebe S, Caro J. On comparing permeation through Matrimid®-based mixed matrix and multilayer sandwich FAU membranes: H_2/CO_2 separation, support functionalization and ion exchange. *Int J Hydrogen Energy*. 2017;42(1):279-288.
39. Dong J, Lin Y. In situ synthesis of P-type zeolite membranes on porous α-alumina supports. *Ind Eng Chem Res*. 1998;37(6):2404-2409.
40. Bondareva G, Rat'ko A, Azarov S. Hydrothermal synthesis of zeolite NaX on porous ceramic supports. *Inorg Mater*. 2003;39(6):605-609.
41. Yang S, Vlessidis AG, Evmiridis NP. Influence of gel composition and crystallization conditions on the conventional synthesis of zeolites. *Ind Eng Chem Res*. 1997;36(5):1622-1631.
42. Ryu J, Ku SH, Lee H, Park CB. Mussel-inspired polydopamine coating as a universal route to hydroxyapatite crystallization. *Adv Funct Mater*. 2010;20(13):2132-2139.
43. Lakshminarayanan R, Madhavi S, Sim CPC. Oxidative polymerization of dopamine: a high-definition multifunctional coatings for electrospun nanofibers-an overview. *Dopamine - Health and Disease*. London: IntechOpen. 2018:113-132.
44. Ravenelle RM, Schüβler F, D'Amico A, et al. Stability of zeolites in hot liquid water. *J Phys Chem C*. 2010;114(46):19582-19595.
45. Zhang L, Chen K, Chen B, White JL, Resasco DE. Factors that determine zeolite stability in hot liquid water. *J Am Chem Soc*. 2015;137(36):11810-11819.
46. Guo S, Yu C, Gu X, Jin W, Zhong J, C-l C. Simulation of adsorption, diffusion, and permeability of water and ethanol in NaA zeolite membranes. *J Membr Sci*. 2011;376(1–2):40-49.
47. Zhang Y, Chen S, Shi R, Du P, Qiu X, Gu X. Pervaporation dehydration of acetic acid through hollow fiber supported DD3R zeolite membrane. *Sep Purif Technol*. 2018;204:234-242.
48. Petushkov A, Freeman J, Larsen SC. Framework stability of nanocrystalline NaY in aqueous solution at varying pH. *Langmuir*. 2010;26(9):6695-6701.
49. Ennaert T, Geboers J, Gobechiya E, et al. Conceptual frame rationalizing the self-stabilization of H-USY zeolites in hot liquid water. *ACS Catal*. 2015;5(2):754-768.
50. Groen JC, Peffer LA, Moulijn JA, Pérez-Ramírez J. Mechanism of hierarchical porosity development in MFI zeolites by desilication: the role of aluminium as a pore-directing agent. *Chem–Eur J*. 2005;11(17):4983-4994.
51. Lutz W, Gessner W, Bertram R, Pitsch I, Fricke R. Hydrothermally resistant high-silica Y zeolites stabilized by covering with non-framework aluminum species. *Microporous Mater*. 1997;12(1–3):131-139.
52. Mokaya R. Al content dependent hydrothermal stability of directly synthesized aluminosilicate MCM-41. *J Phys Chem B*. 2000;104(34):8279-8286.
53. Li Y, Zhou H, Zhu G, Liu J, Yang W. Hydrothermal stability of LTA zeolite membranes in pervaporation. *J Membr Sci*. 2007;297(1–2):10-15.
54. Iskandar F, Zen NA, Mayangsari TR, Aimon AH, Pramana AA. Development of faujasite-type zeolite and iron oxide as mixed catalyst for aquathermolysis reaction of heavy oil. *Mater Res Expr*. 2019;6(4):045510.
55. Król M, Minkiewicz J, Mozgawa W. IR spectroscopy studies of zeolites in geopolymeric materials derived from kaolinite. *J Mol Struct*. 2016;1126:200-206.
56. Liu Z, Ohsuna T, Sato K, et al. Transmission electron microscopy observation on fine structure of zeolite NaA membrane. *Chem Mater*. 2006;18(4):922-927.
57. Hartman RL, Fogler HS. Understanding the dissolution of zeolites. *Langmuir*. 2007;23(10):5477-5484.
58. Zhang Y, Qiu X, Hong Z, Du P, Song Q, Gu X. All-silica DD3R zeolite membrane with hydrophilic-functionalized surface for efficient and highly-stable pervaporation dehydration of acetic acid. *J Membr Sci*. 2019;581:236-242.

SUPPORTING INFORMATION

Additional supporting information may be found online in the Supporting Information section at the end of this article.

How to cite this article: Zhu F, Landon J, Liu K. FAU zeolite membranes for dewatering of amine-based post-combustion CO_2 capture solutions. *AIChE J*. 2020;66:e17042. https://doi.org/10.1002/aic.17042